ELSEVIER

J. Non-Newtonian Fluid Mech. 145 (2007) 15–29

Journal of Non-Newtonian Fluid Mechanics

www.elsevier.com/locate/jnnfm

Upscaling the flow of generalised Newtonian fluids through anisotropic porous media

L. Orgéas [a,*], C. Geindreau [a], J.-L. Auriault [a], J.-F. Bloch [b]

[a] *Laboratoire Sols-Solides-Structures (3S), CNRS, Universités de Grenoble (INPG-UJF), BP 53, 38041 Grenoble Cedex 9, France*
[b] *Laboratoire de Génie des Procédés Papetiers (LGP2), CNRS-INPG-EFPG, BP 65, 461 rue de la Papeterie, 38402 Saint-Martin-d'Hères Cedex 9, France*

Received 16 February 2007; received in revised form 30 March 2007; accepted 7 April 2007

Abstract

The homogenisation method with multiple scale expansions is used to investigate the slow and isothermal flow of generalised Newtonian fluids through anisotropic porous media. From this upscaling it is shown that the first-order macroscopic pressure gradient can be defined as the gradient of a macroscopic viscous dissipation potential, with respect to the first-order volume averaged fluid velocity. The macroscopic dissipation potential is the volume-averaged of local dissipation potential. Using this property, guidelines are proposed to build macroscopic tensorial permeation laws within the framework defined by the theory of anisotropic tensor functions and by using macroscopic isodissipation surfaces. A quantitative numerical study is then performed on a 3D fibrous medium and with a Carreau–Yasuda fluid in order to illustrate the theoretical results deduced from the upscaling.

Keywords: Generalised Newtonian fluid; Porous media; Anisotropy; Homogenisation

1. Introduction

Understanding and modelling the flow of non-Newtonian fluids through porous media is of major importance in many biological systems or processes of the petroleum, pharmaceutical, food, cosmetic, textile, paper and polymer composite industries. The flowing fluids involved in the above application fields usually display complex behaviour, which can exhibit shear thinning/thickening effects, elasticity, anisotropy, yield stress, evolving substructures ... In order to better understand the above complex fluid flows, previous studies have mainly focused on flows through isotropic porous media or on on-axis flows through regular arrangements of parallel cylinders. Considered fluids are generalised Newtonian fluids (see the review of [1]), yield stress fluids [2–4] and viscoelastic fluids [5,6]. In general, the resulting macroscopic flow laws look like modified versions of the isotropic or 1D Darcy's law [7]: the relationship between the macroscopic pressure gradient and the seepage velocity is similar to the constitutive relation between the shear stress and strain rate in the flowing fluid at the pore scale [8].

However, porous media involved in industrial processes or biological systems often exhibit structural anisotropy, and flowing conditions are rarely parallel with the symmetry planes or axes of the porous microstructures. For such situations, the flow of non-Newtonian fluids through these media becomes more problematic. Corresponding tensorial macroscopic flow laws are rare, even for fluids which rheology is slightly more complex than that of Newtonian, i.e. for the generalised Newtonian fluids. As a first step towards the study of more sophisticated fluids, more recent works have analysed numerically slow off-axis flows of some incompressible "simple" inelastic fluids through elementary anisotropic fibrous media [9–12,4,13]. The anisotropy of the macroscopic flow law was found to depend on an intricate coupling between the fibrous microstructure and the rheology of the flowing fluid. For instance, the transverse flow law through a square arrangement of parallel circular cylinders displayed isotropy for Newtonian fluids, whereas it can exhibit significant tetratropy for power-law fluids [10]. Similar trends have been discussed concerning the flow of a shear thinning fluid through regular arrangements of equal capillaries [8]. Hence, from their numerical results, Wodds et al. [9] have

* Corresponding author. Tel.: +33 476 827 073; fax: +33 4 76 82 70 43.
E-mail address: Laurent.Orgeas@hmg.inpg.fr (L. Orgéas).

0377-0257/$ – see front matter © 2007 Elsevier B.V. All rights reserved.
doi:10.1016/j.jnnfm.2007.04.018

first proposed an orthotropic macroscopic flow law for the 2D transverse creeping flow of power-law fluids through rectangular arrays of parallel fibres with elliptical cross sections. More recently, we have pursued their work, extending the domain of validity of their model. We have also tried to provide a methodology to build macroscopic tensorial flow laws of power-law fluids through 2D orthotropic fibrous media: permeation models have been established studying numerically, i.e. empirically, macroscopic isodissipation curves resulting from the pore scale flow [13]. In this paper, we would like (i) to consolidate the above methodology and (ii) to see whether it can be well-suited to other viscous fluids flowing through any anisotropic 3D porous media:

- The pore scale slow flow of a large set of generalised Newtonian fluids (Section 2) is considered and upscaled using the method of homogenisation with multiple scale expansions [14,15](Section 3). Notice that this method has already been used to determine the structure and properties of macroscopic balance and constitutive equations for slow flows of Newtonian fluids [16], power-law fluids [17–19] but also Bingham fluids through porous media [20]. Also notice that other types of upscaling techniques have also been already used to analyse the problem, such as for example the volume averaging method [21–25]. Here, the homogenisation method was chosen because it provides us (i) restrictions to be fulfilled by the considered fluids an equivalent macroscopic description to be possible, and (ii) theoretical results from which key properties of the macroscopic flow law can be further explored (Section 4).
- It is proved theoretically that the macroscopic viscous drag force **f**, which characterises the local fluid resistance to the flow, can be seen as the gradient of a macroscopic viscous dissipation potential $\langle \Phi \rangle$, with respect to the first-order macroscopic seepage velocity $\langle \mathbf{v}^{(0)} \rangle$ (Section 4.1):

$$\mathbf{f} = -\frac{\partial \langle \Phi \rangle}{\partial \langle \mathbf{v}^{(0)} \rangle}.$$

- This important property is useful for the development of macroscopic permeation laws: as examples, 3D tensorial forms of the macroscopic flow laws are proposed when porous media exhibit orthotropy, transverse isotropy or isotropy, within the framework proposed by the theory of anisotropic tensor functions [26–29].
- The last section illustrates the theoretical developments carried out in previous sections. Hence, the pore scale flow of a Carreau–Yasuda fluid through a 3D rectangular arrangement of fibres with elliptical cross sections is first simulated with a finite element code. Numerical results are then used build isodissipation surfaces, from which a macroscopic orthotropic permeation law is identified.

2. Fluid flow description at the pore scale

2.1. Problem statement

As shown in Fig. 1, the porous medium is considered as a periodic assembly of a Representative Elementary Volume (REV) of the porous microstructure. The REV occupies a total volume Ω_{rev} of typical length l_{rev}. The considered REV is made of a rigid solid phase of volume Ω_{s}, which is saturated by a non-Newtonian fluid of volume Ω_{l}. A no-slip boundary condition on the fluid-solid interface Γ is assumed:

$$\mathbf{v} = \mathbf{0} \quad \text{on } \Gamma, \tag{1}$$

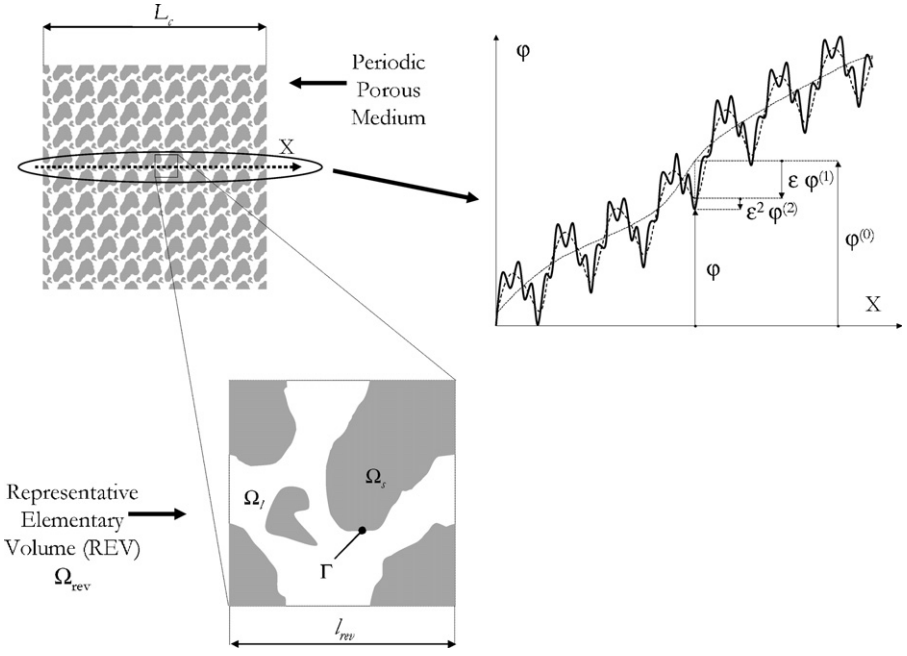

Fig. 1. The porous medium is seen as a periodic assembly of a Representative Elementary Volume (REV). Basic principles of the approximation of a scalar field φ along an arbitrary X axis using asymptotic expansions (here up to the second order).

v being the fluid velocity field. Likewise, the fluid is supposed to be incompressible, isotropic and purely viscous. The mass and momentum balances for an isothermal steady slow flow (inertial effects are neglected) of such an incompressible viscous fluid are respectively:

$$\nabla \cdot \mathbf{v} = 0 \quad \text{in } \Omega_l, \tag{2}$$

$$\nabla \cdot \boldsymbol{\tau} = \nabla p \quad \text{in } \Omega_l. \tag{3}$$

where ∇ is the differential operator with respect to the physical space variable $\mathbf{X}$, p is the incompressibility pressure and where $\boldsymbol{\tau}$ is the viscous stress tensor. $\boldsymbol{\tau}$ is supposed to be a unique function of the strain rate tensor $\mathbf{D} = (\nabla\mathbf{v} + {}^{\mathrm{T}}\nabla\mathbf{v})/2$. In this work, we will focus on the cases where

$$\boldsymbol{\tau} = 2\eta\mathbf{D}, \tag{4}$$

where the fluid viscosity $\eta > 0$ is supposed to be a function of the *equivalent shear strain rate* $\dot{\gamma}_{\mathrm{eq}} = \sqrt{2\mathbf{D} : \mathbf{D}}$. We restrict the present study to the case where

$$\frac{\partial \eta}{\partial \dot{\gamma}_{\mathrm{eq}}} \dot{\gamma}_{\mathrm{eq}} > -\eta. \tag{5}$$

Many well-known rheological models satisfy (4) and (5), the most famous being the Newtonian fluid, shear thinning or thickening versions of the power-law (Ostwald–deWaele) fluid, the Cross fluid or the Carreau–Yasuda fluid [30,31]. . . Let us remark that the purely viscous models that have been developed in order to mimic the viscoplastic Bingham and Herschel–Bulkley models also belong to this group, such as the bi-viscosity model proposed by Lipscomb and Denn [32,33,2,4], the continuous viscous model proposed by Papanastasiou [34,3].

It must be pointed out that for all the viscous fluids under consideration, the viscous stress tensor $\boldsymbol{\tau}$ can be defined as the gradient, with respect to the strain rate tensor $\mathbf{D}$, of a viscous dissipation potential Φ:

$$\boldsymbol{\tau} = \frac{\partial \Phi}{\partial \mathbf{D}}, \tag{6}$$

where the viscous dissipation potential Φ is positive and such that

$$\left.\frac{\partial \Phi}{\partial \mathbf{D}}\right|_{\mathbf{D}=\mathbf{0}} = \boldsymbol{\tau}(\mathbf{D} = \mathbf{0}) = \mathbf{0}. \tag{7}$$

The dissipation potential Φ can also be expressed as a function of $\dot{\gamma}_{\mathrm{eq}}$ so that

$$\boldsymbol{\tau} = \frac{\partial \Phi}{\partial \mathbf{D}} = \frac{\partial \Phi}{\partial \dot{\gamma}_{\mathrm{eq}}} \frac{\partial \dot{\gamma}_{\mathrm{eq}}}{\partial \mathbf{D}} = \tau_{\mathrm{eq}} \frac{\partial \dot{\gamma}_{\mathrm{eq}}}{\partial \mathbf{D}} = 2\frac{\tau_{\mathrm{eq}}}{\dot{\gamma}_{\mathrm{eq}}}\mathbf{D} = 2\eta\mathbf{D}. \tag{8}$$

In the last equation, $\tau_{\mathrm{eq}} = \eta\dot{\gamma}_{\mathrm{eq}}$ is the *equivalent shear stress*. The equivalent shear stress τ_{eq} and the equivalent shear strain rate $\dot{\gamma}_{\mathrm{eq}}$ verify:

$$\mathcal{P}_{\mathrm{dis}} = \boldsymbol{\tau} : \mathbf{D} = 2\eta\mathbf{D} : \mathbf{D} = \eta\dot{\gamma}_{\mathrm{eq}}^2 = \tau_{\mathrm{eq}}\dot{\gamma}_{\mathrm{eq}}, \tag{9}$$

where $\mathcal{P}_{\mathrm{dis}}$ is the volumetric mechanical dissipation. Finally, it is important to notice that restriction (5) implies that the dissipation potential Φ is convex:

$$\forall\, \mathbf{D}_a, \mathbf{D}_b \in E_3 \otimes E_3, \quad \Phi(\mathbf{D}_b) - \Phi(\mathbf{D}_a) \geq \left.\frac{\partial \Phi}{\partial \mathbf{D}}\right|_a : (\mathbf{D}_b - \mathbf{D}_a). \tag{10}$$

2.2. Separation of scales

In order to obtain a macroscopic description of the above local physics, it is assumed, as illustrated in Fig. 1, that the geometrical length l_{rev} as well as the characteristic local length l_c of the physical phenomena under consideration are supposed to be small compared to the characteristic length L_c of the sample or macroscopic excitation. By assuming (for a sake of simplicity) that l_{rev} and l_c are of the same order of magnitude, such a scale separation condition is directly connected to the scale separation parameter ε, that must be small for a macroscopic equivalent model to exist:

$$\varepsilon = \frac{l_c}{L_c} \ll 1, \tag{11}$$

- For the considered fluid flow problem, the local length l_c can be seen as the characteristic thickness of the sheared fluid at the pore scale. As an example, by considering the in-axis transverse flow of power-law fluids through rectangular arrangement of parallel cylinders with an elliptical cross section, the characteristic length is found to be close to half the gap between two neighbouring fibres [9,13].
- In case of a laboratory permeation experiment performed with an homogeneous porous sample and under homogenous testing conditions (e.g. constant pressure gradient), the macroscopic length L_c is typically the height of the sample. For more complex situations, i.e. in case of a permeation problem trough a porous medium displaying macroscopic heterogeneities (varying upon a characteristic length L_h) and subjected to a macroscopic heterogeneous loading (e.g. pressure gradient varying upon a characteristic length L_p), the macroscopic length L_c would be the smallest length between L_h and L_p.

2.3. Dimensionless pore scale description

Adopting the methodology proposed in [35], we introduce in Eqs. (1) and (2) the following dimensionless variables (subscript "c" denotes characteristic values)

$$\mathbf{y}^* = \frac{1}{l_c}\mathbf{X}, \qquad \mathbf{v}^* = \frac{1}{v_c}\mathbf{v}, \qquad p^* = \frac{p}{\Delta p_c}, \qquad \mathbf{D}^* = \frac{l_c}{v_c}\mathbf{D},$$
$$\boldsymbol{\tau}^*(\mathbf{D}^*) = \frac{1}{\tau_c}\boldsymbol{\tau}. \tag{12}$$

The vector $\mathbf{y}^*$ is the so-called non-dimensional *microscopic space variable*: it is obtained normalizing $\mathbf{X}$ using the characteristic length l_c. In the above dimensionless variables, pressure and deviatoric stresses have been distinguished, because they are associated with two different physical phenomena. The pressure p, which typical variation in the considered problem is Δp_c, is

directly connected with the fluid incompressibility constraint (2). By contrast, shear stresses, of characteristic value τ_c, are induced by viscous deviatoric deformation of the fluid during the flow. Hence, the formal dimensionless set of equations that describes the flow is thus written

$$\begin{cases} \nabla^* \cdot \mathbf{v}^* = 0 & \text{in } \Omega_1^* \\ \nabla^* \cdot \boldsymbol{\tau}^* = \mathcal{Q}\nabla^* p^* & \text{in } \Omega_1^* \\ \mathbf{v}^* = \mathbf{0} & \text{on } \Gamma^*, \end{cases} \tag{13}$$

where ∇^* is the dimensionless gradient operator with respect to the microscopic space variable $\mathbf{y}^*$ and where

$$\boldsymbol{\tau}^* = 2\eta^*(\dot{\gamma}_{\text{eq}}^*)\mathbf{D}^* \tag{14}$$

and

$$\mathcal{Q} = \frac{\Delta p_c}{\tau_c}. \tag{15}$$

The order of magnitude of the dimensionless number $\mathcal{Q}$ can be estimated. For instance, during a permeation experiment performed with an homogeneous porous sample of height L_c and under homogenous testing conditions, the fluid flow is driven by a balance between local volumetric viscous drag forces of characteristic value $f_c = \tau_c/l_c$, and the imposed macroscopic pressure gradient of characteristic value $\Delta p_c/L_c$ [35,19]:

$$\frac{\Delta p_c}{L_c} = \mathcal{O}(f_c) = \mathcal{O}\left(\frac{\tau_c}{l_c}\right). \tag{16}$$

so that

$$\mathcal{Q} = \mathcal{O}(\varepsilon^{-1}), \tag{17}$$

Hence, it is possible to rewrite the local dimensionless description as

$$\begin{cases} \nabla^* \cdot \mathbf{v}^* = 0 & \text{in } \Omega_1^* \\ \varepsilon\nabla^* \cdot \boldsymbol{\tau}^* = \nabla^* p^* & \text{in } \Omega_1^* \\ \mathbf{v}^* = \mathbf{0} & \text{on } \Gamma^*. \end{cases} \tag{18}$$

3. Upscaling

The homogenisation procedure is then achieved by introducing the multiple scale coordinates [14,15]: the macroscopic dimensionless space variable, $\mathbf{x}^* = \mathbf{X}/L_c$, and the microscopic dimensionless space variable $\mathbf{y}^*$, both being linked by $\mathbf{x}^* = \varepsilon\mathbf{y}^*$. If (11) is well-satisfied, then $\mathbf{y}^*$ and $\mathbf{x}^*$ can be considered as two independent space variables, and the physical variables of the problem, i.e. the velocity and the pressure, can then be seen as *a priori* functions of $\mathbf{y}^*$ and $\mathbf{x}^*$, i.e. $\mathbf{v}^*(\mathbf{y}^*) = \mathbf{v}^*(\mathbf{x}^*, \mathbf{y}^*)$ and $p^*(\mathbf{y}^*) = p^*(\mathbf{x}^*, \mathbf{y}^*)$. Consequently, the spatial differential operator ∇^* can be written as

$$\nabla^* = \nabla_{y^*} + \frac{l_c}{L_c}\nabla_{x^*} = \nabla_{y^*} + \varepsilon\nabla_{x^*}. \tag{19}$$

where ∇_{y^*} and ∇_{x^*} represent spatial differential operators with respect to $\mathbf{y}^*$ and $\mathbf{x}^*$, respectively. As illustrated by the graph plotted in Fig. 1, we now assume that the velocity and pressure fields can be expressed in the form of asymptotic expansions in powers of ε [14,15]:

$$\begin{aligned} \mathbf{v}^* &= \mathbf{v}^{*(0)}(\mathbf{x}^*, \mathbf{y}^*) + \varepsilon\mathbf{v}^{*(1)}(\mathbf{x}^*, \mathbf{y}^*) + \varepsilon^2\mathbf{v}^{*(2)}(\mathbf{x}^*, \mathbf{y}^*) + \cdots, \\ p^* &= p^{*(0)}(\mathbf{x}^*, \mathbf{y}^*) + \varepsilon p^{*(1)}(\mathbf{x}^*, \mathbf{y}^*) + \varepsilon^2 p^{*(2)}(\mathbf{x}^*, \mathbf{y}^*) + \cdots, \end{aligned} \tag{20}$$

where the functions $\mathbf{v}^{*(i)}$ and $p^{*(i)}$ are of the same order of magnitude and are supposed to be Ω-periodic with respect to the dimensionless space variable $\mathbf{y}^*$. By noting

$$\begin{aligned} \forall i \geq 0, \quad \mathbf{D}_y^{*(i)} &= \frac{\nabla_{y^*}\mathbf{v}^{*(i)} + {}^{\mathrm{T}}\nabla_{y^*}\mathbf{v}^{*(i)}}{2}, \\ \mathbf{D}_x^{*(i)} &= \frac{\nabla_{x^*}\mathbf{v}^{*(i)} + {}^{\mathrm{T}}\nabla_{x^*}\mathbf{v}^{*(i)}}{2} \end{aligned} \tag{21}$$

and

$$\mathbf{D}^{*(0)} = \mathbf{D}_y^{*(0)}, \qquad \mathbf{D}^{*(i)} = \mathbf{D}_x^{*(i-1)} + \mathbf{D}_y^{*(i)}, \quad i > 0, \tag{22}$$

and then

$$\begin{aligned} \dot{\gamma}_{\text{eq}}^{*(0)} &= \sqrt{2\mathbf{D}^{*(0)} : \mathbf{D}^{*(0)}}, \qquad \dot{\gamma}_{\text{eq}}^{*(1)} = \sqrt{4\mathbf{D}^{*(0)} : \mathbf{D}^{*(1)}}, \\ \dot{\gamma}_{\text{eq}}^{*(2)} &= \sqrt{2\mathbf{D}^{*(1)} : \mathbf{D}^{*(1)} + 4\mathbf{D}^{*(0)} : \mathbf{D}^{*(2)}}, \end{aligned} \tag{23}$$

the dimensionless strain rate tensor $\mathbf{D}^*$ and shear strain rate $\dot{\gamma}_{\text{eq}}^*$ involved in (14) now respectively become

$$\mathbf{D}^* = \mathbf{D}^{*(0)} + \varepsilon\mathbf{D}^{*(1)} + \varepsilon^2\mathbf{D}^{*(2)} + \cdots, \tag{24}$$

$$\dot{\gamma}_{\text{eq}}^{*2} = \dot{\gamma}_{\text{eq}}^{*(0)^2} + \varepsilon\dot{\gamma}_{\text{eq}}^{*(1)^2} + \varepsilon^2\dot{\gamma}_{\text{eq}}^{*(2)^2} + \cdots \tag{25}$$

The viscosity η^* is then expressed as a Taylor expansion around $\dot{\gamma}_{\text{eq}}^{*(0)}$.

$$\begin{aligned} \eta^*(\dot{\gamma}_{\text{eq}}^*) = \eta^*(\dot{\gamma}_{\text{eq}}^{*(0)}) &+ \left[\frac{\partial\eta^*}{\partial\dot{\gamma}_{\text{eq}}^{*2}}\right]_{\dot{\gamma}_{\text{eq}}^{*(0)}} \varepsilon(\dot{\gamma}_{\text{eq}}^{*(1)^2} + \varepsilon\dot{\gamma}_{\text{eq}}^{*(2)^2} + \cdots) + \cdots \\ &+ \left[\frac{\partial^k\eta^*}{\partial(\dot{\gamma}_{\text{eq}^{*2}})^k}\right]_{\dot{\gamma}_{\text{eq}}^{*(0)}} \frac{1}{k!}\varepsilon^k(\dot{\gamma}_{\text{eq}}^{*(1)^2} + \varepsilon\dot{\gamma}_{\text{eq}}^{*(2)^2} + \cdots)^k + \cdots \end{aligned} \tag{26}$$

By assuming that

$$\forall k \geq 1, \quad \mathcal{O}\left(\frac{1}{k!}\left|\left[\frac{\partial^k\eta^*}{\partial(\dot{\gamma}_{\text{eq}}^{*2})^k}\right]_{\dot{\gamma}_{\text{eq}}^{*(0)}}\right|\right) \leq \mathcal{O}(\varepsilon^{1-k}), \tag{27}$$

the viscosity η^* can then be put in the form:

$$\eta^* = \eta^{*(0)} + \varepsilon\eta^{*(1)} + \varepsilon^2\eta^{*(2)} + \cdots, \tag{28}$$

where the $\eta^{*(i)}$'s are of the same order of magnitude. Assumption (27) ensures that $\eta^{*(0)} = \eta^*(\dot{\gamma}_{\text{eq}}^{*(0)})$. This is a necessary condition for the problem to be homogenisable. From a physical point of view, this means that within the neighbouring of $\dot{\gamma}_{\text{eq}}^{*(0)}$, the variation of η^* with $\dot{\gamma}_{\text{eq}}^*$ must not be too sharp. Under such circumstances, the viscous stress tensor can be expanded as

$$\boldsymbol{\tau}^* = \boldsymbol{\tau}^{*(0)} + \varepsilon\boldsymbol{\tau}^{*(1)} + \varepsilon^2\boldsymbol{\tau}^{*(2)} + \cdots \tag{29}$$

where the $\boldsymbol{\tau}^{*(i)}$ are of the same order of magnitude and where, in particular,

$$\boldsymbol{\tau}^{*(0)} = 2\eta^{*(0)}\mathbf{D}^{*(0)} = \boldsymbol{\tau}^*(\mathbf{D}^{*(0)}). \tag{30}$$

The method then consists in incorporating the above expansions in the dimensionless system (18) and identifying the successive orders of ε. At the lowest (zero) order one obtains:

$$\begin{cases} \nabla_{y^*} \cdot \mathbf{v}^* = 0 & \text{in } \Omega_1^* \\ \nabla_{y^*} p^{*(0)} = 0 & \text{in } \Omega_1^* \\ \mathbf{v}^{*(0)} = \mathbf{0} & \text{on } \Gamma^* \end{cases} \tag{31}$$

At the next order, the following set of equations is obtained:

$$\begin{cases} \nabla_{x^*} \cdot \mathbf{v}^{*(0)} + \nabla_{y^*} \cdot \mathbf{v}^{*(1)} = 0 & \text{in } \Omega_1^*, \\ \nabla_{y^*} \cdot \boldsymbol{\tau}^*(\mathbf{D}^{*(0)}) = \nabla_{y^*} p^{*(1)} + \nabla_{x^*} p^{*(0)} & \text{in } \Omega_1^*, \\ \mathbf{v}^{*(1)} = \mathbf{0} & \text{on } \Gamma^*. \end{cases} \tag{32}$$

3.1. First-order pressure

From (31b) it is concluded that

$$p^{*(0)}(\mathbf{x}^*, \mathbf{y}^*) = p^{*(0)}(\mathbf{x}^*), \tag{33}$$

so that at the first order, the pressure does not depend on the local space variable $\mathbf{y}^*$, i.e. $p^{*(0)}$ is constant in the whole REV.

3.2. Self-equilibrium of the REV

The set of Eqs. (31a), (31c), (32c) represents a boundary value problem for the $\mathbf{y}^*$-periodic unknowns $\mathbf{v}^{*(0)}$ and $p^{*(1)}$, in which the macroscopic pressure gradient $\nabla_{x^*} p^{*(0)}$ is considered as a known and constant volumetric source term (at this stage of the homogenisation process). The corresponding weak formulation is

$$\forall\, \mathbf{u}^* \in \mathbb{H}, \quad \int_{\Omega_1^*} \boldsymbol{\tau}^*(\mathbf{D}^{*(0)}) : \mathbf{D}_y^*(\mathbf{u}^*)\, \mathrm{d}V^* + \int_{\Omega_1^*} \mathbf{u}^* \cdot \nabla_{x^*} p^{*(0)}\, \mathrm{d}V^* = 0, \tag{34}$$

where $\mathbb{H}$ is a Hilbert space of vectors $\mathbf{u}^*$ defined on Ω_1^*, $\mathbf{y}^*$-periodic, divergence free and zero-valued over Γ^*. To obtain (34), $\mathbb{H}$ was ascribed the following inner product:

$$(\mathbf{u}^*, \mathbf{v}^*)_{\mathbb{H}} = \int_{\Omega_1^*} \nabla_{y^*}\mathbf{u}^* : \nabla_{y^*}\mathbf{v}^*\, \mathrm{d}V^*. \tag{35}$$

Adopting a reasoning similar to that proposed in [19] in the case of power-law fluids, the convexity property (10) as well as the last equation are used to obtain the following variational inequality:

$$\forall\, \mathbf{w}^* \in \mathbb{H}, \quad \mathcal{J}(\mathbf{w}^*) - \mathcal{J}(\mathbf{v}^{*(0)}) \geq 0, \tag{36}$$

where $\mathcal{J}$ is a convex function defined as

$$\mathcal{J}(\mathbf{w}^*) = \int_{\Omega_1^*} (\Phi^*(\mathbf{D}_y^*(\mathbf{w}^*)) + \mathbf{w}^* \cdot \nabla_{x^*} p^{*(0)})\, \mathrm{d}V^*. \tag{37}$$

There exists a unique solution $\mathbf{w}^* \in \mathbb{H}$ that minimizes $\mathcal{J}(\mathbf{w}^*)$, i.e. $\mathbf{w}^* = \mathbf{v}^{*(0)}$. This solution depends on the microscopic space variable $\mathbf{y}^*$, the macroscopic gradient of pressure $\nabla_{x^*} p^{*(0)}$, the rheology of the fluid (rheo), and the porous medium microstructure (micro):

$$\mathbf{v}^{*(0)} = \mathbf{v}^{*(0)}(\nabla_{x^*} p^{*(0)},\ \text{rheo}, \text{micro}) \tag{38}$$

Accounting for the last result, (32b) now shows that $p^{*(1)}$ is also a function $p'^{*(1)}$ of the imposed macroscopic pressure gradient $\nabla_{x^*} p^{*(0)}$, up to an arbitrary $\mathbf{y}$-independent pressure $p''^{*(1)}(\mathbf{x})$:

$$p^{*(1)} = p'^{*(1)}(\nabla_{x^*} p^{*(0)},\ \text{rheo}, \text{micro}) + p''^{*(1)}(\mathbf{x}) \tag{39}$$

In practice (e.g. the numerical example exposed in Section 5), the pressure $p''^{*(1)}$ can arbitrarily be set to 0 on only one point of the REV.

3.3. Macroscopic balance equations of the flow

The integration of the mass balance equation (32a) over Ω_1^*, combined with both the periodicity boundary condition and the no-slip boundary condition (32c) on Γ^* yield the following compatibility condition, here recasted in a dimensional form:

$$\nabla \cdot \langle \mathbf{v}^{(0)} \rangle = 0 \quad \text{in } \Omega_1, \tag{40}$$

with

$$\langle \mathbf{v}^{(0)} \rangle = \frac{1}{\Omega_{\text{rev}}} \int_{\Omega_1} \mathbf{v}^{(0)}\, \mathrm{d}V = \mathbf{h}(\nabla p^{(0)},\ \text{rheo}, \text{micro}), \tag{41}$$

or, in the reverse form:

$$\nabla p^{(0)} = \mathbf{f}(\langle \mathbf{v}^{(0)} \rangle,\ \text{rheo}, \text{micro}), \tag{42}$$

where $\mathbf{f}$ is here seen as a volumetric viscous drag force. Eqs. (40) and (42) represents respectively the macroscopic mass and momentum balance equations for the macroscopic equivalent continuous medium, within an order $\mathcal{O}(\varepsilon)$ approximation. Moreover, choosing $\mathbf{u}^* = \mathbf{v}^{*(0)}$ in (34) yields:

$$\int_{\Omega_1^*} \mathcal{P}_{\text{dis}}(\mathbf{D}^{(0)}(\mathbf{v}^{(0)}))\, \mathrm{d}V + \int_{\Omega_1} \mathbf{v}^{(0)} \cdot \nabla p^{(0)}\, \mathrm{d}V = 0, \tag{43}$$

which shows that the first-order macroscopic volumetric dissipation, *i.e.* $-\nabla p^{(0)} \cdot \langle \mathbf{v}^{(0)} \rangle = -\mathbf{f} \cdot \langle \mathbf{v}^{(0)} \rangle$, equals the first-order volume average $\langle \mathcal{P}_{\text{dis}} \rangle$ of local dissipative source $\mathcal{P}_{\text{dis}}$:

$$-\mathbf{f} \cdot \langle \mathbf{v}^{(0)} \rangle = \frac{1}{\Omega} \int_{\Omega_1} \mathcal{P}_{\text{dis}}\, \mathrm{d}V = \langle \mathcal{P}_{\text{dis}} \rangle = \langle \tau_{\text{eq}} \dot{\gamma}_{\text{eq}} \rangle. \tag{44}$$

4. Structure and property of the macroscopic flow law

4.1. General form

When the flowing fluid is Newtonian, relation (34) proves that the drag force $\mathbf{f}$ is a linear function of $\langle \mathbf{v}^{(0)} \rangle$, so that Eq. (42) reduces to a general Darcy's law. When the power-law model is used, Eq. (34) shows that $\mathbf{f}$ is an homogeneous function of degree n of $\langle \mathbf{v}^{(0)} \rangle$ [17–19], n being the power-law exponent of the flowing fluid. For other considered viscous models, no similar

specific property can be established. Hence, in order to further investigate the general form of the macroscopic flow law for these fluids, i.e. the relation between $\mathbf{f}$ and $\langle\mathbf{v}^{(0)}\rangle$, the volume average $\langle\Phi\rangle$ of the dissipation potential Φ is introduced:

$$\langle\Phi\rangle = \frac{1}{\Omega}\int_{\Omega_l}\Phi(\mathbf{D}(\mathbf{v}^{(0)}))\,\mathrm{d}V. \tag{45}$$

$\langle\Phi\rangle$ is convex and positive. The variation $\mathrm{d}\langle\Phi\rangle$ of $\langle\Phi\rangle$ can be written as

$$\begin{aligned}\mathrm{d}\langle\Phi\rangle &= \frac{1}{\Omega}\int_{\Omega_l}(\Phi(\mathbf{D}(\mathbf{v}^{(0)}+\mathrm{d}\mathbf{v}^{(0)})) - \Phi(\mathbf{D}(\mathbf{v}^{(0)})))\,\mathrm{d}V\\ &= \frac{1}{\Omega}\int_{\Omega_l}\frac{\partial\Phi}{\partial\mathbf{D}^{(0)}} : \mathbf{D}(\mathrm{d}\mathbf{v}^{(0)})\,\mathrm{d}V + \cdots\\ &= \frac{1}{\Omega}\int_{\Omega_l}\boldsymbol{\tau}(\mathbf{D}^{(0)}) : \mathbf{D}(\mathrm{d}\mathbf{v}^{(0)})\,\mathrm{d}V + \cdots\end{aligned} \tag{46}$$

or, by putting $\mathbf{u}^* = \mathrm{d}\mathbf{v}^{*(0)}$ in (34):

$$\mathrm{d}\langle\Phi\rangle = -\mathbf{f}\cdot\frac{1}{\Omega}\int_{\Omega_l}\mathrm{d}\mathbf{v}^{(0)}\,\mathrm{d}V + \cdots. \tag{47}$$

If we now suppose that $\langle\Phi\rangle$ can be expressed as a function of $\langle\mathbf{v}^{(0)}\rangle$, *i.e.* $\langle\Phi\rangle = \langle\Phi\rangle(\langle\mathbf{v}^{(0)}\rangle)$, it is possible to write:

$$\begin{aligned}\mathrm{d}\langle\Phi\rangle &= \langle\Phi\rangle(\langle\mathbf{v}^{(0)}\rangle + \mathrm{d}\langle\mathbf{v}^{(0)}\rangle) - \langle\Phi\rangle(\langle\mathbf{v}^{(0)}\rangle)\\ &= \frac{\partial\langle\Phi\rangle}{\partial\langle\mathbf{v}^{(0)}\rangle}\cdot\mathrm{d}\langle\mathbf{v}^{(0)}\rangle + \cdots\end{aligned} \tag{48}$$

Therefore, as $\mathrm{d}\mathbf{v}^{(0)} \to \mathbf{0}$, Eqs. (47) and (46) allow us to write by identification:

$$\mathbf{f} = -\frac{\partial\langle\Phi\rangle}{\partial\langle\mathbf{v}^{(0)}\rangle} \tag{49}$$

so that the drag force $\mathbf{f}$ is the gradient, with respect to $\langle\mathbf{v}^{(0)}\rangle$, of a macroscopic dissipation potential defined as the volume average $\langle\Phi\rangle$ of the local dissipation potential Φ. As a consequence, the drag force $\mathbf{f}$ obeys the normality rule: when it is plotted in the velocity space, $\mathbf{f}$ is normal to the iso-potential surface passing through the point which position is defined by $\langle\mathbf{v}^{(0)}\rangle$. Such a property was recently emphasized numerically (empirically) in the case of 2D flow of power-law fluids through fibrous media [13].

At the microscopic scale, we have shown in Section 2 that Φ could be expressed as a function of the local *equivalent shear strain rate* $\dot\gamma_{\mathrm{eq}}$. Similarly, it is assumed that at the macroscopic scale, $\langle\Phi\rangle$ can be expressed as a function of an *equivalent velocity* $v_{\mathrm{eq}}(\langle\mathbf{v}^{(0)}\rangle)$, defined as a norm in the velocity space. Hence, a more convenient form of the drag force $\mathbf{f}$ is obtained:

$$\mathbf{f} = -\frac{\partial\langle\Phi\rangle}{\partial v_{\mathrm{eq}}}\frac{\partial v_{\mathrm{eq}}}{\partial\langle\mathbf{v}^{(0)}\rangle} = -f_{\mathrm{eq}}\frac{\partial v_{\mathrm{eq}}}{\partial\langle\mathbf{v}^{(0)}\rangle}, \tag{50}$$

where

$$f_{\mathrm{eq}} = \frac{\partial\langle\Phi\rangle}{\partial v_{\mathrm{eq}}} \tag{51}$$

is the *equivalent drag force*. f_{eq} and v_{eq} both verify:

$$\langle\mathcal{P}_{\mathrm{dis}}\rangle = \langle\tau_{\mathrm{eq}}\dot\gamma_{\mathrm{eq}}\rangle = -\mathbf{f}\cdot\langle\mathbf{v}^{(0)}\rangle = f_{\mathrm{eq}}v_{\mathrm{eq}}. \tag{52}$$

Lastly, by accounting for the physical arguments used to establish (16), the equivalent drag force may be expressed as

$$f_{\mathrm{eq}} = \frac{\tau_{\mathrm{c}}}{l_{\mathrm{c}}}. \tag{53}$$

From (4) and (12), we get

$$\tau_{\mathrm{c}} = \eta\frac{v_{\mathrm{c}}}{l_{\mathrm{c}}} \quad \text{with } \eta = \eta\left(\frac{v_{\mathrm{c}}}{l_{\mathrm{c}}}\right). \tag{54}$$

Introducing α, a constitutive parameter that links the characteristic local velocity v_{c} with the macroscopic equivalent velocity v_{eq} by $v_{\mathrm{c}} = \alpha v_{\mathrm{eq}}$, leads finally to another form of f_{eq}:

$$f_{\mathrm{eq}} = \frac{1}{l_{\mathrm{c}}}\eta\frac{\alpha v_{\mathrm{eq}}}{l_{\mathrm{c}}} = f(v_{\mathrm{eq}}) \quad \text{with } \eta = \eta\left(\frac{\alpha v_{\mathrm{eq}}}{l_{\mathrm{c}}}\right). \tag{55}$$

Notice that due to restriction (5) imposed on the viscosity η, the function f can be inverted (see Section 4.5). Likewise, taking into account (55), the macroscopic dissipation may be expressed as

$$\langle\mathcal{P}_{\mathrm{dis}}\rangle = f_{\mathrm{eq}}v_{\mathrm{eq}} = \frac{\alpha}{l_{\mathrm{c}}^2}\eta v_{\mathrm{eq}}^2 \quad \text{with } \eta = \eta\left(\frac{\alpha v_{\mathrm{eq}}}{l_{\mathrm{c}}}\right). \tag{56}$$

Consequently, when it is plotted in the velocity space, the macroscopic isodissipation surface corresponds to a constant equivalent velocity. Moreover, the form of the general macroscopic flow law of viscous fluids under consideration through any anisotropic rigid porous media now reads

$$\mathbf{f} = -\frac{\alpha}{l_{\mathrm{c}}^2}\eta v_{\mathrm{eq}}\frac{\partial v_{\mathrm{eq}}}{\partial\langle\mathbf{v}^{(0)}\rangle} \quad \text{with } \eta = \eta\left(\frac{\alpha v_{\mathrm{eq}}}{l_{\mathrm{c}}}\right). \tag{57}$$

In the next three sections, the expression of v_{eq} will be further specified for cases where the porous microstructures display orthotropy, transverse isotropy and isotropy.

4.2. Orthotropic porous media

4.2.1. General form

When the considered porous medium displays at least two orthogonal symmetry planes of unit normals $\mathbf{e}_{\mathrm{I}}$ and $\mathbf{e}_{\mathrm{II}}$ (for instance), i.e. when it exhibits orthotropy with three orthogonal axes $\mathbf{e}_{\mathrm{I}}$, $\mathbf{e}_{\mathrm{II}}$ and $\mathbf{e}_{\mathrm{III}} = \mathbf{e}_{\mathrm{I}} \times \mathbf{e}_{\mathrm{II}}$, standard results of the theory of representation of anisotropic tensor functions allows us to express $\mathbf{f}$ by the following frame-independent form (for details, see [26–29]):

$$\mathbf{f} = -(\varphi_{\mathrm{I}}\mathbf{M}_{\mathrm{I}} + \varphi_{\mathrm{II}}\mathbf{M}_{\mathrm{II}} + \varphi_{\mathrm{III}}\mathbf{M}_{\mathrm{III}})\cdot\langle\mathbf{v}^{(0)}\rangle, \tag{58}$$

where the $\mathbf{M}_i$'s are microstructure tensors defined as (no summation on the indices i):

$$\mathbf{M}_i = \mathbf{e}_i\otimes\mathbf{e}_i, \quad i = \mathrm{I, II, III}, \tag{59}$$

and where the scalar rheological functions φ_i may depend on the studied microstructure, the rheology of the flowing fluid and on the following velocity invariants, here written in a tensorial frame-independent form:

$$V_i = \sqrt{\langle \mathbf{v}^{(0)} \rangle \cdot \mathbf{M}_i \cdot \langle \mathbf{v}^{(0)} \rangle}, \quad i = \mathrm{I, II, III}. \tag{60}$$

For example, when the macroscopic velocity field $\langle \mathbf{v}^{(0)} \rangle$ is expressed in the principal reference frame $(\mathbf{e}_\mathrm{I}, \mathbf{e}_\mathrm{II}, \mathbf{e}_\mathrm{III})$, the invariant V_i corresponds to the absolute value of the principal velocity component, i.e. to $|\langle v_i^{(0)} \rangle|$. Therefrom, by accounting for (57) and (58) the general form of the macroscopic permeation law through orthotropic porous media can be put in the form

$$\mathbf{f} = -\frac{\alpha}{l_\mathrm{c}^2} \eta v_\mathrm{eq} \left(\frac{1}{V_\mathrm{I}} \frac{\partial v_\mathrm{eq}}{\partial V_\mathrm{V}} \mathbf{M}_\mathrm{I} + \frac{1}{V_\mathrm{II}} \frac{\partial v_\mathrm{eq}}{\partial V_\mathrm{II}} \mathbf{M}_\mathrm{II} + \frac{1}{V_\mathrm{III}} \frac{\partial v_\mathrm{eq}}{\partial V_\mathrm{III}} \mathbf{M}_\mathrm{III} \right) \cdot \langle \mathbf{v}^{(0)} \rangle, \tag{61}$$

in which v_eq depends on the three velocity invariants (60) and where $\eta = \eta(\alpha v_\mathrm{eq}/l_\mathrm{c})$.

4.2.2. Expression for v_{eq}

When the flowing fluid is Newtonian ($\eta = \eta_0$) the last relation, when combined with the momentum balance (42), must lead to the Darcy's law

$$\nabla p^{(0)} = -\eta_0 \left(\frac{1}{k_\mathrm{I}} \mathbf{M}_\mathrm{I} + \frac{1}{k_\mathrm{II}} \mathbf{M}_\mathrm{II} + \frac{1}{k_\mathrm{III}} \mathbf{M}_\mathrm{III} \right) \cdot \langle \mathbf{v}^{(0)} \rangle, \tag{62}$$

where the k_i's are the principal values of the permeability tensor. They are constant. This results in the following constraint for the equivalent velocity v_eq:

$$\frac{v_\mathrm{eq}}{V_i} \frac{\partial v_\mathrm{eq}}{\partial V_i} = \mathrm{cst}, \quad i = \mathrm{I,II,II}, \quad \text{no summation} \tag{63}$$

Therefore, v_eq may be put in the following quadratic form

$$v_\mathrm{eq}^2 = V_\mathrm{I}^2 + \left(\frac{V_\mathrm{II}}{A} \right)^2 + \left(\frac{V_\mathrm{III}}{B} \right)^2, \tag{64}$$

up to an arbitrary multiplicative constant (here we set it to 1). The strictly positive and constant constitutive parameters A and B depend on the microstructure. They are directly connected to the anisotropy of the flow in the principal directions: for a given macroscopic mechanical dissipation, *i.e.* for a given equivalent velocity v_eq, the macroscopic velocity components equal $\langle v_\mathrm{I}^{(0)} \rangle \mathbf{e}_\mathrm{I}$, $(\langle v_\mathrm{I}^{(0)} \rangle / A) \mathbf{e}_\mathrm{II}$ and $(\langle v_\mathrm{I}^{(0)} \rangle / B) \mathbf{e}_\mathrm{III}$ in the $\mathbf{e}_\mathrm{I}$, $\mathbf{e}_\mathrm{II}$ and $\mathbf{e}_\mathrm{III}$ directions, respectively. As a consequence, it follows from (61), (62) and (64) that

$$k_\mathrm{I} = \frac{l_\mathrm{c}^2}{\alpha}, \qquad k_\mathrm{II} = \frac{(A l_\mathrm{c})^2}{\alpha}, \qquad k_\mathrm{III} = \frac{(B l_\mathrm{c})^2}{\alpha}. \tag{65}$$

For non-Newtonian fluids, the equivalent velocity v_eq must fulfil the two following constraints: (i) it must be convex with respect to the V_i's, in order to ensure the convexity of $\langle \Phi \rangle$, and (ii) it must be such that any imposed velocity field $\langle \mathbf{v}^{(0)} \rangle$ contained in a symmetry plane of normal $\mathbf{e}_i$ ($i \in \{\mathrm{I,II,II}\}$) results in a viscous drag force $\mathbf{f}$ that is also contained in this plane. In other words (no summation on the index i):

$$\forall\, i \in \{\mathrm{I,II,III}\}, \quad \left. \frac{\partial v_\mathrm{eq}}{\partial V_i} \right|_{V_i = 0} = 0. \tag{66}$$

Within such a framework, different forms of v_eq may be proposed. For example, in order to describe the 2D in-plane flow of power-law fluids through orthotropic fibrous media, the following 2D form v_eqa was proposed [13]:

$$v_\mathrm{eqa}^{m_\mathrm{a}} = V_\mathrm{I}^{m_\mathrm{a}} + \left(\frac{V_\mathrm{II}}{A} \right)^{m_\mathrm{a}}. \tag{67}$$

This expression of v_eq introduces two additional constitutive parameters m_a and A. The form that is proposed here for 3D flows through orthotropic porous media is

$$v_\mathrm{eq}^m = v_\mathrm{eqa}^m + v_\mathrm{eqb}^m, \tag{68}$$

where

$$v_\mathrm{eqa}^{m_\mathrm{a}} = V_\mathrm{I}^{m_\mathrm{a}} + \left(\frac{V_\mathrm{II}}{A} \right)^{m_\mathrm{a}}, \qquad v_\mathrm{eqb} = \frac{V_\mathrm{III}}{B},$$
$$m = \frac{m_\mathrm{b} V_\mathrm{I}^2 + m_\mathrm{c} V_\mathrm{II}^2}{V_\mathrm{I}^2 + V_\mathrm{II}^2}. \tag{69}$$

Such a proposition involves five constitutive parameters A, B, m_a, m_b and m_c that may depend on the microstructure of the porous medium and on the rheology of the flowing fluid. In order to ensure the convexity of $\langle \Phi \rangle$, m_a, m_b and m_c are assumed to belong to $]1; +\infty[$. To ensure the linearity of the flow law when the fluid rheology tends to that of a Newtonian fluid, m_a, m_b and m_c must tend towards 2, in accordance with (64). Notice that the form of v_eq given in (68) and (69) reduce to the 2D form v_eqa proposed in (67) when the imposed velocity field belongs to the $(\mathbf{e}_\mathrm{I}, \mathbf{e}_\mathrm{II})$ plane. Fig. 2 depicts the shapes of the isodissipation surfaces, i.e. the equivalent velocity surfaces in the velocity invariant space, for particular values of m_a, m_b, m_c, A and B. This figure also shows that A and B characterize the anisotropy of the surfaces v_eq, whereas m_a, m_b and m_c control their curvatures. Using (68) and (69) yields:

$$\frac{\partial v_\mathrm{eq}}{\partial V_\mathrm{I}} = \frac{m_{,V_\mathrm{I}}}{m} v_\mathrm{eq} \left(\left(\frac{v_\mathrm{eqb}}{v_\mathrm{eq}} \right)^m \ln v_\mathrm{eqb} + \left(\frac{v_\mathrm{eqa}}{v_\mathrm{eq}} \right)^m \times \left(\ln v_\mathrm{eqa} + \frac{m}{m_{,V_\mathrm{I}}} \frac{V_\mathrm{I}^{m_\mathrm{a}-1}}{v_\mathrm{eqa}^{m_\mathrm{a}}} \right) - \ln v_\mathrm{eq} \right),$$
$$\frac{\partial v_\mathrm{eq}}{\partial V_\mathrm{II}} = \frac{m_{,V_\mathrm{II}}}{m} v_\mathrm{eq} \left(\left(\frac{v_\mathrm{eqb}}{v_\mathrm{eq}} \right)^m \ln v_\mathrm{eqb} + \left(\frac{v_\mathrm{eqa}}{v_\mathrm{eq}} \right)^m \times \left(\ln v_\mathrm{eqa} + \frac{m}{A^{m_\mathrm{a}} m_{,V_\mathrm{II}}} \frac{V_\mathrm{II}^{m_\mathrm{a}-1}}{v_\mathrm{eqa}^{m_\mathrm{a}}} \right) - \ln v_\mathrm{eq} \right),$$
$$\frac{\partial v_\mathrm{eq}}{\partial V_\mathrm{III}} = \frac{1}{B^m} \left(\frac{V_\mathrm{III}}{v_\mathrm{eq}} \right)^{m-1}, \tag{70}$$

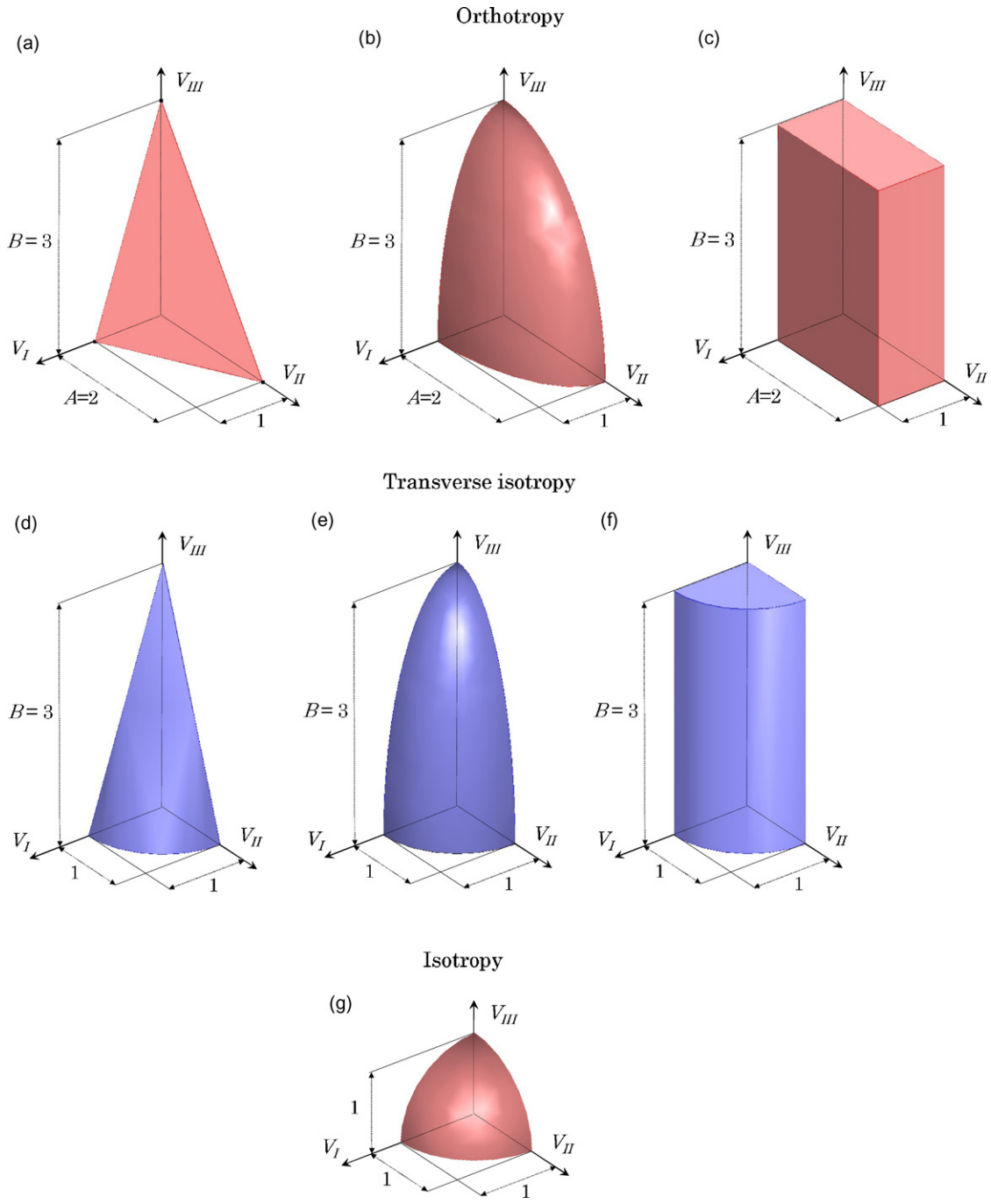

Fig. 2. Possible shapes of isopotential surfaces v_{eq} plotted in the (V_I, V_{II}, V_{III}) space. Orthotropy, v_{eq} is given by (68) with $A = 2$ and $B = 3$ (arbitrary units): $m_a = m_b = m_c \to 1$ (a), $m_a = m_b = m_c = 2$ (b) and $m_a = m_b = m_c \to \infty$ (c). Transverse isotropy, v_{eq} is given by (76) with $B = 3$: $m \to 1$ (d), $m = 2$ (e) and $m \to \infty$ (f). (g): Isotropy, v_{eq} is given by (80) and reduces to the Euclidian norm.

where

$$m_{,V_I} = \frac{\partial m}{\partial V_I} = \frac{2(m_b - m_c)V_I V_{II}^2}{(V_I^2 + V_{II}^2)^2},$$
$$m_{,V_{II}} = \frac{\partial m}{\partial V_{II}} = \frac{2(m_c - m_b)V_I^2 V_{II}}{(V_I^2 + V_{II}^2)^2}. \quad (71)$$

Hence, the viscous drag force $\mathbf{f}$ can now be estimated from (61), when the values of l_c, α, A, B, m_a, m_b and m_c are given.

4.3. Transversely isotropic porous media

When the considered porous medium displays transverse isotropy, which axis is for example $\mathbf{e}_{III}$, $\mathbf{f}$ takes the form:

$$\mathbf{f} = -(\varphi\mathbf{M} + \varphi_{III}\mathbf{M}_{III}) \cdot \langle \mathbf{v}^{(0)} \rangle, \quad (72)$$

where

$$\mathbf{M} = \mathbf{M}_I + \mathbf{M}_{II}, \quad (73)$$

and where the scalar rheological functions φ and φ_{III} depend on V_{III} and

$$V = \sqrt{\langle \mathbf{v}^{(0)} \rangle \cdot \mathbf{M} \cdot \langle \mathbf{v}^{(0)} \rangle} = \sqrt{V_I^2 + V_{II}^2}. \tag{74}$$

A general form of the macroscopic permeation law through transversely isotropic porous media is

$$\mathbf{f} = -\frac{\alpha}{l_c^2}\eta \left(\frac{v_{eq}}{V}\frac{\partial v_{eq}}{\partial V}\mathbf{M} + \frac{v_{eq}}{V_{III}}\frac{\partial v_{eq}}{\partial V_{III}}\mathbf{M}_{III} \right) \cdot \langle \mathbf{v}^{(0)} \rangle. \tag{75}$$

in which v_{eq} depends on V and V_{III} and where $\eta = \eta(\alpha v_{eq}/l_c)$. The following form of v_{eq}:

$$v_{eq}^m = V^m + \left(\frac{V_{III}}{B} \right)^m \tag{76}$$

is proposed to complete the macroscopic model. As previously, the parameter m belongs to $]1;+\infty[$. The various possible and admissible shapes of isodissipation surfaces (76) are sketched in Fig. 2, and the macroscopic flow law becomes

$$\mathbf{f} = -\frac{\alpha}{l_c^2}\eta \left(\left(\frac{V}{v_{eq}} \right)^{m-2} \mathbf{M} + \frac{1}{B^m}\left(\frac{V_{III}}{v_{eq}} \right)^{m-2} \mathbf{M}_{III} \right) \cdot \langle \mathbf{v}^{(0)} \rangle. \tag{77}$$

where $\eta = \eta(\alpha v_{eq}/l_c)$. When the fluid is Newtonian, $m = 2$ and (77) becomes

$$\mathbf{f} = -\eta_0 \left(\frac{1}{k_\perp}\mathbf{M} + \frac{1}{k_\parallel}\mathbf{M}_{III} \right) \cdot \langle \mathbf{v}^{(0)} \rangle, \tag{78}$$

where the principal transverse $k_\perp$ and on-axis $k_\parallel$ permeabilities are expressed as

$$k_\perp = \frac{l_c^2}{\alpha}, \quad k_\parallel = \frac{(Bl_c)^2}{\alpha}. \tag{79}$$

4.4. Isotropic porous media

When the considered porous media have no preferred direction, the permeation law is isotropic, i.e. it is invariant to any given rotation of the macroscopic flow with respect to the porous medium. In this case, v_{eq} simply reduces to the Euclidian norm (see Fig. 2):

$$v_{eq} = \| \langle \mathbf{v}^{(0)} \rangle \|, \tag{80}$$

and the permeation law (57) can now be written as

$$\mathbf{f} = -\frac{\alpha}{l_c^2}\eta \langle \mathbf{v}^{(0)} \rangle \quad \text{with} \quad \eta = \eta \left(\frac{\alpha \| \langle \mathbf{v}^{(0)} \rangle \|}{l_c} \right). \tag{81}$$

If the fluid is Newtonian, the last relation as well as the momentum balance equation (42) yield to the well-known isotropic Darcy's law:

$$\nabla p^{(0)} = -\frac{\eta_0}{k}\langle \mathbf{v}^{(0)} \rangle, \tag{82}$$

where $k = l_c^2/\alpha$ is the permeability of the considered porous medium.

4.5. Reverse form of the macroscopic flow law

For practical reasons, it may be more convenient to express the macroscopic permeation law (49) in a reverse form, i.e. $\langle \mathbf{v}^{(0)} \rangle = \langle \mathbf{v}^{(0)} \rangle(\mathbf{f})$. As a matter of fact, by accounting for (42), i.e. $\mathbf{f} = \nabla p^{(0)}$, it is then possible to introduce this reverse form in (40). This leads to a well-posed non-linear boundary values problem at the macroscale in terms of $p^{(0)}$only, when providing a proper set of associated boundary conditions. For that purpose, we introduce the complementary volumetric dissipation potential $\langle \Phi_c \rangle(\mathbf{f})$ with the following Legendre transform [36]:

$$\langle \Phi_c \rangle(\mathbf{f}) = \max_{\langle \mathbf{v} \rangle} \{ -\mathbf{f} \cdot \langle \mathbf{v} \rangle - \langle \Phi \rangle(\langle \mathbf{v} \rangle) \}. \tag{83}$$

The convexity of $\langle \Phi \rangle$ shows then that relation (83) is equivalent to

$$\langle \Phi_c \rangle(\mathbf{f}) = -\mathbf{f} \cdot \langle \mathbf{v}^{(0)} \rangle - \langle \Phi \rangle(\langle \mathbf{v}^{(0)} \rangle) = \langle \mathcal{P}_{dis} \rangle - \langle \Phi \rangle(\langle \mathbf{v}^{(0)} \rangle) \tag{84}$$

Therewith, it is concluded that the reverse form of (49) is

$$\langle \mathbf{v}^{(0)} \rangle = -\frac{\partial \langle \Phi_c \rangle}{\partial \mathbf{f}}. \tag{85}$$

The macroscopic velocity $\langle \mathbf{v}^{(0)} \rangle$ is then the gradient of $\langle \Phi_c \rangle$ with respect to $\mathbf{f}$. Adopting a reasoning similar to that introduced in Section 4.1, it is possible to express (85) as

$$\langle \mathbf{v}^{(0)} \rangle = -v_{eq}\frac{\partial f_{eq}}{\partial \mathbf{f}}, \tag{86}$$

which represents the reverse form of (57) with

$$v_{eq} = \frac{\partial \langle \Phi_c \rangle}{\partial f_{eq}}. \tag{87}$$

The physical meaning of $\langle \Phi \rangle$ and $\langle \Phi_c \rangle$ is illustrated in the graph of Fig. 3. The bold curve plotted in this graph is a possible evolution of the constitutive relation (55). The area below the curve equals the dissipation potential $\langle \Phi \rangle$. The area above the

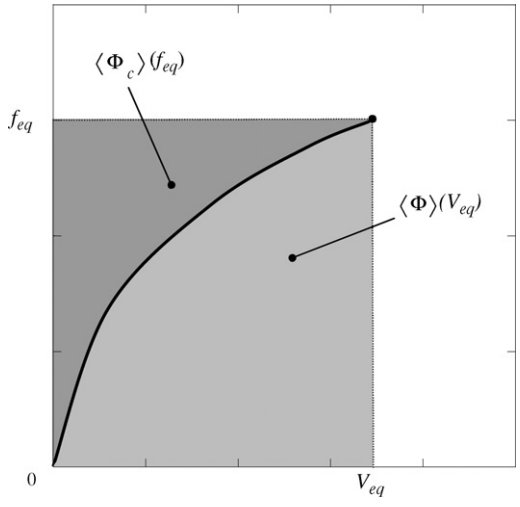

Fig. 3. Schematic graph showing the evolution of the equivalent viscous force f_{eq} as a function of the equivalent velocity v_{eq}. This graph also illustrates the physical meaning of $\langle \Phi \rangle$ and $\langle \Phi_c \rangle$

curve equals the dissipation potential $\langle \Phi_c \rangle$. The sum of these two areas equals the mechanical dissipation $\langle \mathcal{P}_{dis} \rangle$, in accordance with (52) and (84).

By returning to (86) and by adopting a reasoning identical to that conducted in the three previous subsections, the following expressions of f_{eq} are proposed:

- Orthotropic porous media

$$f_{eq}^{m'} = f_{eqa}^{m'} + f_{eqb}^{m'}, \tag{88}$$

with

$$f_{eqa}^{m'_a} = F_I^{m'_a} + \left(\frac{F_{II}}{A'}\right)^{m'_a}, \qquad f_{eqb} = \frac{F_{III}}{B'},$$

$$m' = \frac{m'_b F_I^2 + m'_c F_{II}^2}{F_I^2 + F_{II}^2}. \tag{89}$$

- Transversely isotropic porous media

$$f_{eq}^{m'} = F^{m'} + \left(\frac{F_{III}}{B'}\right)^{m'}. \tag{90}$$

- Isotropic porous media

$$f_{eq} = \|\mathbf{f}\|. \tag{91}$$

In relations (88)–(90) we have noted

$$F_i = \sqrt{\mathbf{f} \cdot \mathbf{M}_i \cdot \mathbf{f}}, \quad i = \text{I,II,II}, \tag{92}$$

and

$$F = \sqrt{F_I^2 + F_{II}^2}. \tag{93}$$

Considering on-axis flows, it can be easily shown that $A' = 1/A$ and $B' = 1/B$. For transverse isotropy, it is also possible to show without major difficulty that $m' = m/(m-1)$. For orthotropy and if $m'_b = m'_c$, one obtains $m'_a = m_a/(m_a - 1)$, and $m'_b = m_b/(m_b - 1)$. For general orthotropy, it can be shown that $m'_a = m_a/(m_a - 1)$, $m'_b = m_b/(m_b - 1)$ and $m'_c = m_c/(m_c - 1)$ when the flow is contained in $(\mathbf{e}_I, \mathbf{e}_{II})$, $(\mathbf{e}_I, \mathbf{e}_{III})$ and $(\mathbf{e}_{II}, \mathbf{e}_{III})$ planes, respectively. For other types of flow, we have shown from numerical simulations that the last relations could still be considered as valid, at least for the considered orthotropic microstructures (see next section).

5. Illustration

In order to illustrate the theoretical developments of the previous sections, the flow a generalised Newtonian fluid through an elementary periodic orthotropic fibrous medium (Section 5.1) is studied from numerical simulations. Hence, the associated REV is subjected to a macroscopic pressure gradient $\nabla p^{(0)}$ and the local velocity field $\mathbf{v}^{(0)}$ is computed from the self-equilibrium of the REV (Section 5.2). This allows to identify the constitutive parameters α, l_c, A, B, m_a, m_b and m_c of the proposed orthotropic macroscopic flow law (61), (68)(Section 5.3).

5.1. Studied fluid and microstructures

The considered fluid is a Carreau–Yasuda fluid [30,31], which shear viscosity is expressed as

$$\eta = \eta_\infty + (\eta_0 - \eta_\infty)\left(1 + \left(\frac{\dot{\gamma}_{eq}}{\dot{\gamma}_0}\right)^{a_c}\right)^{n-1/a_c}, \tag{94}$$

involving five constitutive parameters, i.e. η_0, η_∞, $\dot{\gamma}_0$, n and a_c we have set here arbitrarily to 1 Pa s, 0 Pa s, 1 s^{-1}, 0.2 and 2, respectively. The Carreau–Yasuda fluid was here chosen because it is often used to model the steady state shear rheology of polymeric solutions. By putting $n = 1$ and $\dot{\gamma}_0 = \tau_0/(\eta_0 - \eta_\infty)$ in (94), also notice that this model can also be well suited as a regularised version of the Bingham model, in a way similar to the bi-viscosity model (with a yield shear stress τ_0, an initial viscosity η_0 and an infinite viscosity η_∞ such as $\eta_0 \gg \eta_\infty$) [32,33,4].

This fluid is flowing across a square array of infinite and parallel fibres with elliptical cross-section. A scheme of the REV is given in Fig. 4. Even if it is very simple, the chosen REV may be rather closed to that of some unidirectional fibre-bundle mats used in polymer composites [37]. It exhibits orthotropy, since it has three orthogonal symmetry planes which unit normals are $\mathbf{e}_I$, $\mathbf{e}_{II}$ and $\mathbf{e}_{III}$. The principal normal vectors $\mathbf{e}_I$, $\mathbf{e}_{II}$ and $\mathbf{e}_{III}$ are supposed to be aligned with the vectors of the reference frame $\mathbf{e}_1$, $\mathbf{e}_2$ and $\mathbf{e}_3$ directions, respectively. The dimensions of the REV are h_I, h_{II} in the $\mathbf{e}_I$ and $\mathbf{e}_{II}$, respectively. Similarly, the major and minor axis of the cross section of the fibre are noted a_I and a_{II} (see Fig. 4). The aspect ratios of the cross sections of both the REV and the fibre are identical, i.e. $h_{II}/h_I = a_{II}/a_I = r$. In this example, we have set $h_I = 1$m and $r = 0.5$. Moreover, the volume fraction of fibre $c = \pi a_I^2/h_I^2$ was arbitrarily set to 0.6.

5.2. Fluid flow computation at the pore scale

To evaluate the constitutive parameters of the macroscopic flow law, it is first necessary to determine the local velocity field $\mathbf{v}^{(0)}$ in the whole REV. As shown in Section 3.2, this can be achieved by solving numerically the dimensional form of the self-equilibrium of the REV (31a), (31c), (32c):

$$\begin{cases} \nabla \mathbf{v}^{(0)} = 0 & \text{in } \Omega_l \\ \nabla p^{(0)} + \nabla \varepsilon p^{(1)} = 2\nabla(\mathbf{D}^{(0)} + (1 + (\dot{\gamma}_{eq}^{(0)})^2)^{-0.4}\,\mathbf{D}^{(0)}) & \text{in } \Omega_l \\ \mathbf{v}^{(0)} = \mathbf{0} & \text{on } \Gamma \end{cases} \tag{95}$$

where the macroscopic pressure gradient $\nabla p^{(0)}$ is given on the entire REV and where the unknowns $\mathbf{v}^{(0)}$ and $\varepsilon p^{(1)}$ are periodic. Notice that the symmetries of the considered REV, fluid and loadings, are such that the previous boundary value problem does not depend on the space variable X_3. Therefore, the calculation of the four unknowns $v_1^{(0)}(X_1, X_2)$, $v_2^{(0)}(X_1, X_2)$, $v_3^{(0)}(X_1, X_2)$ and $\varepsilon p^{(1)}(X_1, X_2)$ can be carried out in the 2D space $(\mathbf{e}_I, \mathbf{e}_{II})$, so reducing considerably the computation time. Practically, this non-linear boundary values problem was solved using the Finite Element software Comsol® [38] with a mixed pressure–velocity

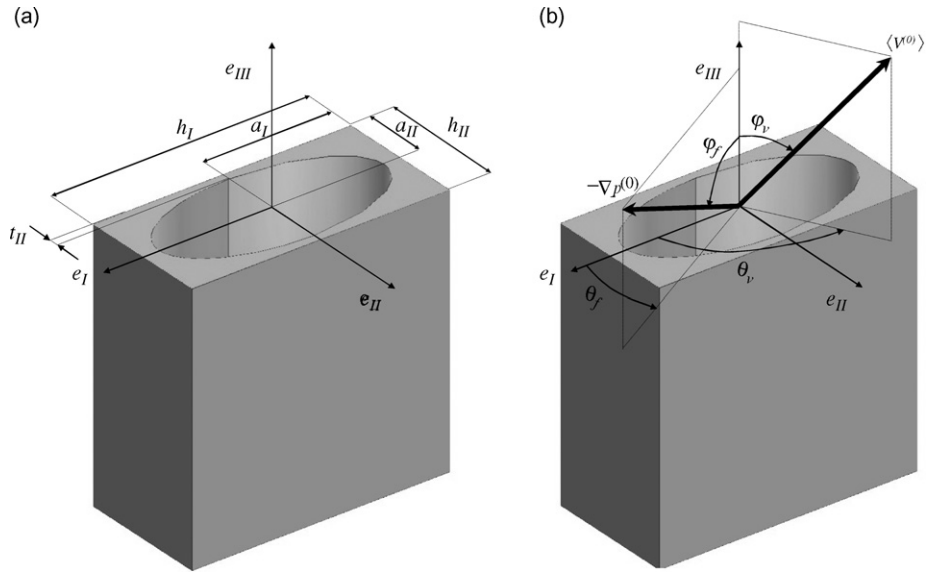

Fig. 4. Scheme of the Representative Elementary Volume of the considered microstructure. Dimensions (a), form of the imposed macroscopic gradient $\nabla p^{(0)}$ and resulting macroscopic velocity field $\langle \mathbf{v}^{(0)} \rangle$ (b).

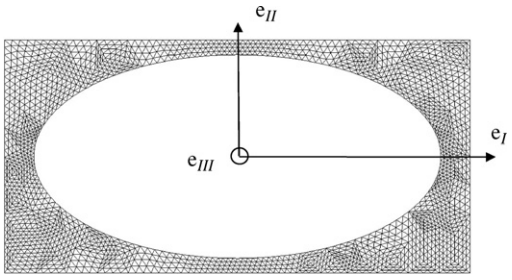

Fig. 5. 2D FE mesh used to run simulations.

(P1–P2) formulation. Fine triangular finite elements were used to mesh the geometry, as depicted in Fig. 5. In order to validate the numerical procedure implemented in Comsol®, at least in the case of the transverse flows of Newtonian and power-law fluids through this type of REV, we have systematically compared our numerical results to previous ones [10,13]. Thereby, the REV is subjected to a macroscopic pressure gradient $\nabla p^{(0)}$ of intensity denoted $\|\nabla p^{(0)}\|$ and such that (Fig. 6):

$$\nabla p^{(0)} = -\|\nabla p^{(0)}\|(\sin\varphi_f \cos\theta_f \mathbf{e}_I + \sin\varphi_f \sin\theta_f \mathbf{e}_{II} + \cos\varphi_f \mathbf{e}_{III}). \quad (96)$$

The corresponding macroscopic velocity $\langle \mathbf{v}^{(0)} \rangle$ is written as

$$\langle \mathbf{v}^{(0)} \rangle = \|\langle \mathbf{v}^{(0)} \rangle\|(\sin\varphi_v \cos\theta_v \mathbf{e}_I + \sin\varphi_v \sin\theta_v \mathbf{e}_{II} + \cos\varphi_v \mathbf{e}_{III}), \quad (97)$$

where the angles θ_f, θ_v, φ_f and φ_v are defined in Fig. 4. An example of calculation is plotted in Fig. 7, for which a unit macroscopic gradient is imposed along the vertical axis, i.e. $\nabla p^{(0)} = -\mathbf{e}_{III}\,(\text{Pa m}^{-1})$ ($\varphi_f = 0$).

5.3. Numerical results

5.3.1. On-axis flows: determination of α, l_c, A and B

In relations (61), (68)–(70), α and l_c characterise on-axis flows along the $\mathbf{e}_I$ direction. In the case of the particular studied microstructure, it is possible to express α as a function of l_c by using a mass balance, i.e. $2l_c v_c = rlv_{eq} \Leftrightarrow \alpha = rl/2l_c = 1/4l_c$. As a consequence, during permeations along the $\mathbf{e}_I$, $\mathbf{e}_{II}$ and $\mathbf{e}_{III}$ directions, the principal drag forces f_I, f_{II} and f_{III} are respectively linked to the principal velocities $\langle v^{(0)} \rangle_I$, $\langle v^{(0)} \rangle_{II}$ and $\langle v^{(0)} \rangle_{III}$

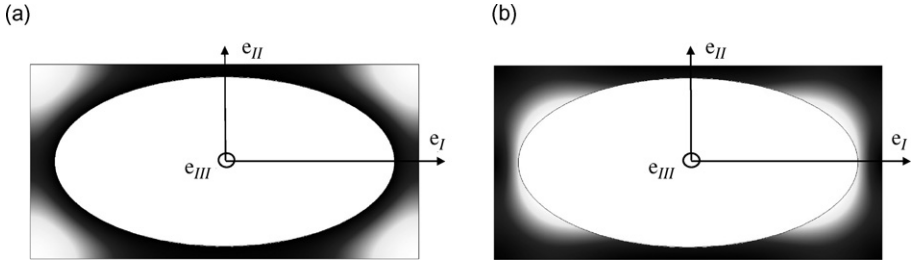

Fig. 6. Example of results—the imposed macroscopic gradient is along the vertical axis, i.e. $\nabla p^{(0)} = -\mathbf{e}_{III}\,(\text{Pa m}^{-1})$. (a) Corresponding norm of the local velocity field $\|\mathbf{v}^{(0)}\|$, the linear gray scale ranges from 0 m s^{-1} (black) to 0.0114 m s^{-1} (white). (b) Corresponding local shear strain rate $\dot{\gamma}_{eq}^{(0)}$, the linear gray scale ranges from 0 s^{-1} (black) to 0.155 s^{-1} (white).

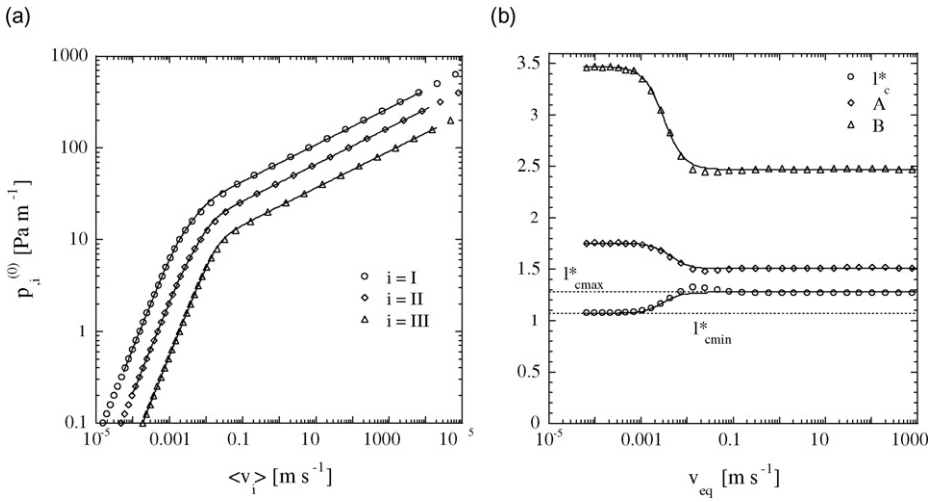

Fig. 7. On-axis flows: (a) Evolution of the imposed macroscopic on-axis pressure gradient $p^{(0)}_{,i}\mathbf{e}_i$ (i = I, II, III, no summation) as a function of the on-axis macroscopic velocity field $\langle v^{(0)}_i\rangle\mathbf{e}_i$ (i = I, II, III, no summation). Marks represent the simulated results. Continuous lines are prediction (98) combined with (99). (b) Evolution of $l^*_c = l_c/t_{II}$, A and B with the equivalent velocity v_{eq}. Marks represent the simulated results. Continuous lines are prediction (99).

by

$$f_I = -\left(1+\left(\frac{|\langle v^{(0)}_I\rangle|}{4l_c^2}\right)^2\right)^{-0.4}\frac{\langle v^{(0)}_{II}\rangle}{4l_c^3},$$

$$f_{II} = -\left(1+\left(\frac{|\langle v^{(0)}_{II}\rangle|}{4Al_c^2}\right)^2\right)^{-0.4}\frac{\langle v^{(0)}_{II}\rangle}{4A^2l_c^3},$$

$$f_{III} = -\left(1+\left(\frac{|\langle v^{(0)}_{III}\rangle|}{4Bl_c^2}\right)^2\right)^{-0.4}\frac{\langle v^{(0)}_{III}\rangle}{4B^2l_c^3}. \quad (98)$$

Therefore, l_c, A and B can be determined from the knowledge of permations performed along the principal directions of the microstructure. This is illustrated in Fig. 7. Marks plotted in Fig. 7(a) of this figure show the evolution of the imposed on-axis pressure gradients $p^{(0)}_{,i}\mathbf{e}_i$ (i = I, II, II, no summation) as a function of the simulated on-axis macroscopic velocity fields $\langle v^{(0)}_i\rangle\mathbf{e}_i$ (i = I, II, III, no summation). For the three on-axis flows, macroscopic pressure gradients follows a "Carreau–Yasuda-like" evolution, in accordance with (98). This graph also clearly reveals the anisotropy of the flow law, as the three curves are far from being superimposed. The graph (b) in Fig. 7 shows the evolution of $l^*_c = l_c/t_{II}$, A and B (deduced from these numerical results and (98)) as functions of v_{eq}, where t_{II} is defined as half the gap between two neighbouring fibres (see Fig. 4). These values display two constant zones, during which the fluid can be considered as a Newtonian fluid and as a power-law fluid ($n = 0.2$), respectively. The two constant zones are linked by a transition zone which occurs more or less at an equivalent velocity $v_{eq} \approx 4\bar{l}_c^2$, where $\bar{l}_c \approx 0.037$ m is defined as $(l_{cmax} + l_{cmin})/2$ (see Fig. 7(b)). Results also show that A and B tends to diminish as v_{eq} increases: for instance, $B \approx 3.5$ and $A \approx 1.75$ in the Newtonian zone, whereas $B \approx 2.48$ and $A \approx 1.51$ in the power-law one. Moreover, one can notice that l_c is of the same order of magitude as t_{II}, as already pointed out in earlier studies [9,13]. Lastly, we have fitted the evolution of l_c, A and B using the following expression:

$$\xi = \bar{\xi} \pm \Delta\xi \tanh\left(\frac{\eta_\xi}{\Delta\xi}\ln\frac{v_{eq}}{v_\xi}\right) \quad (99)$$

where ξ equals l_c, A and B, respectively, and where the values of the constants $\bar{\xi}$, $\Delta\xi$, η_ξ and v_ξ are reported in Table 1. Also shown by the continuous lines plotted in Fig. 7 b, such fits fairly well reproduce the variations of l_c, A and B and allow a good modelling of our numerical on-axis (see the continuous lines plotted in Fig. 7a).

5.3.2. *Off-axis flows: determination of m_a, m_b and m_c*

To estimate m_a, m_b and m_c, isodissipation surfaces $v_{eq}(P_0)$, or $f_{eq}(P_0)$, both corresponding to given values P_0 of the macroscopic mechanical dissipation $\langle\mathcal{P}_{dis}\rangle$, were first determined from numerical results and plotted in the velocity space (V_I, V_{II}, V_{III}), or in the viscous drag force space (F_I, F_{II}, F_{III}). For that purpose:

- numerical simulations were performed with various values of (θ_f, φ_f) : $\varphi_f = 0$ and $0 \le \theta_f \le \pi/2$, $\theta_f = 0$ and $0 \le \varphi_f \le \pi/2$, $\theta_f = \pi/4$ and $0 \le \varphi_f \le \pi/2$, $\theta_f = \pi/2$ and $0 \le$

Table 1
Constant parameters used in Eq. (99) to fit the evolutions of l_c, A, B, m_a, m_b and m_c with v_{eq}.

ξ	$\pm$	$\bar{\xi}$	$\Delta\xi$	η_ξ	v_ξ(m s^{-1})
l_c	+	0.037 m	0.0032 m	0.0032 m	0.003
A	−	1.63	0.125	0.13	0.0043
B	−	2.97	0.5	0.5	0.0031
m_a	−	1.67	0.33	0.24	0.0037
m_b	−	1.75	0.25	0.22	0.004
m_c	−	1.84	0.16	0.09	0.01

$\varphi_f \leq \pi/2, \varphi_f = \pi/2 - \theta_f/2$ and $0 \leq \theta_f \leq \pi/2, \varphi_f = \pi/4 + \theta_f/2$ and $0 \leq \theta_f \leq \pi/2$.

- for given values of (θ_f, φ_f), the norm $\|\nabla p^{(0)}\|$ of the imposed macroscopic pressure gradient was adjusted so that the simulated dissipation $\nabla p^{(0)} \cdot \mathbf{v}^{(0)}$ equals the prescribed dissipation P_0: this was achieved with an elementary dichotomy which was found to converge quite quickly (≈ 10 iterations for a relative precision of 0.1%).

The as-determined numerical isodissipation surfaces $v_{eq}(P_0)$ and $f_{eq}(P_0)$ were respectively fitted with (68) and (88), where the parameters $A = 1/A'$ and $B = 1/B'$ have been already determined (see previous section). From these fits, it was first found that the equalities $m'_a = m_a/(m_a - 1)$, $m'_b = m_b/(m_b - 1)$ and $m'_c = m_c/(m_c - 1)$ are valid. Moreover, as shown in Fig. 8, the best fits of (68) and (88) allow a rather good description of our numerical results, in the Newtonian (Fig. 8(a) and (b)), transition

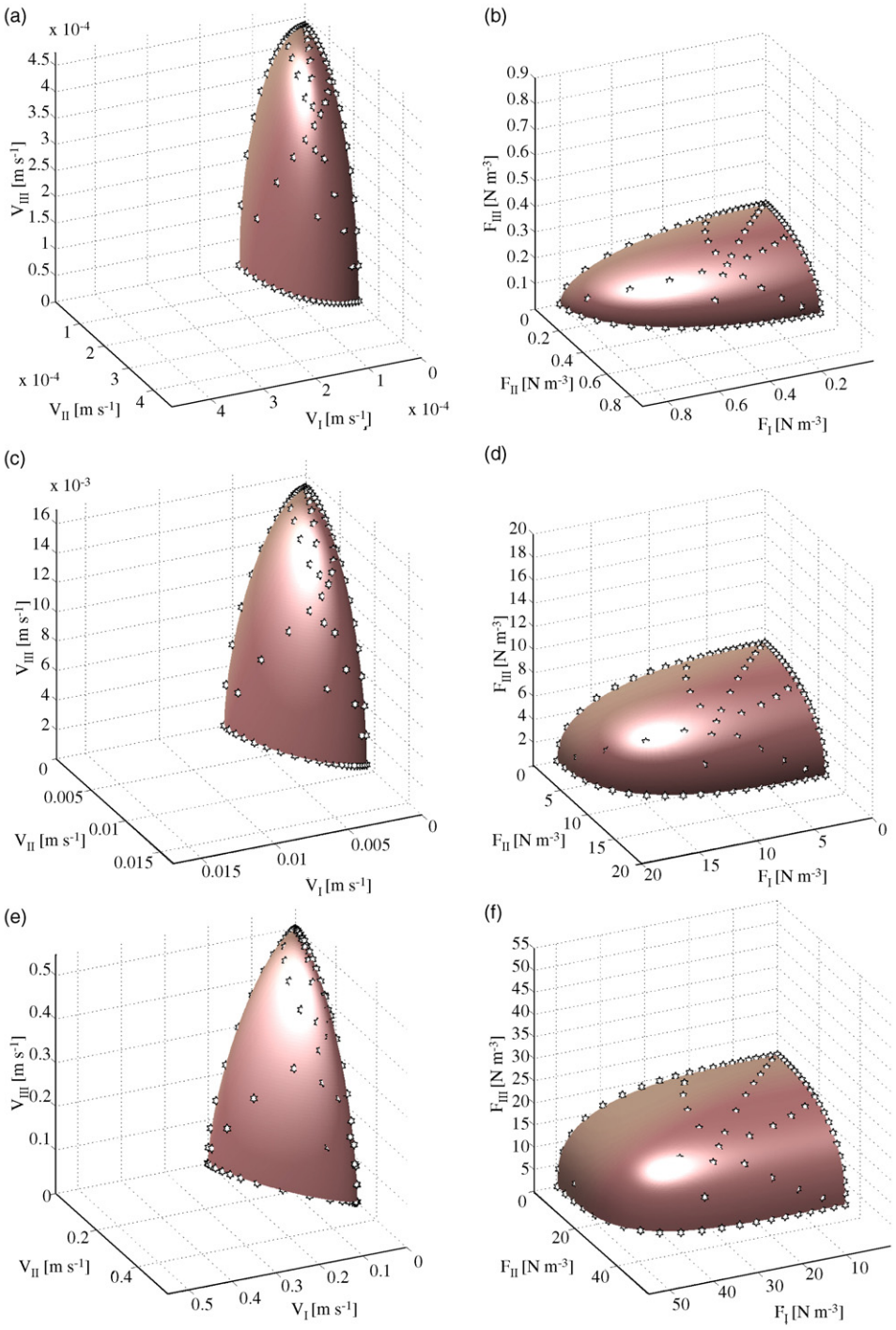

Fig. 8. Numerical (stars) and fitted (continuous surfaces) isodissipation surfaces v_{eq} (a, c and e) and f_{eq} (b, d and f), respectively plotted in the (V_I, V_{II}, V_{III}) and (F_I, F_{II}, F_{III}) invariant spaces. The surfaces have been determined for $P_0 = 10^{-4}$ W m^{-3} or $v_{eq} = 1.256 \times 10^{-4}$ m s^{-1} (a and b), $P_0 = 10^{-1}$ W m^{-3} or $v_{eq} = 5.58 \times 10^{-3}$ m s^{-1} (c and d), and $P_0 = 10^{1}$ W m^{-3} or $v_{eq} = 2.02 \times 10^{-1}$ m s^{-1} (e and f).

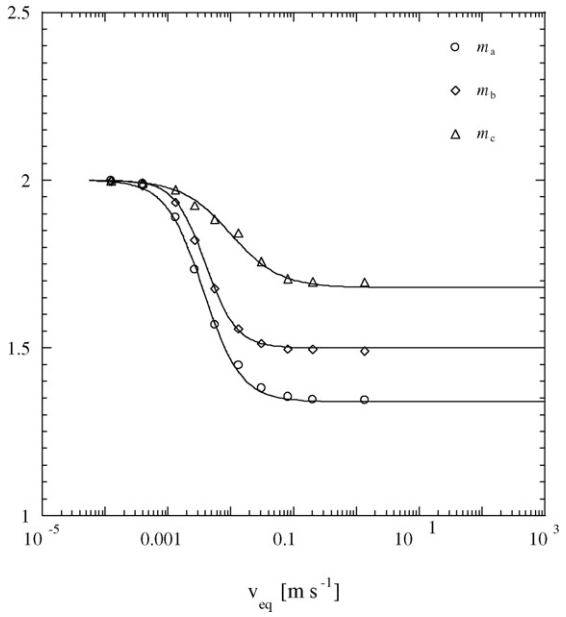

Fig. 9. Evolution of m_a, m_b and m_c with the equivalent velocity v_{eq}. Marks have been determined from the best fits of isodissipation surfaces. Continuous lines are the prediction of the best fits of (99).

(Fig. 8(c) and (d)) or power-law (Fig. 8(e) and (f)) regimes, even if the fits are less satisfactory in this last regime. Fig. 9 shows the evolutions as functions of v_{eq} of the constitutive parameters m_a, m_b and m_c deduced from isodissipation surfaces. As for l_c, A and B, the parameters m_a, m_b and m_c are constant in the Newtonian and power-law regimes. Once again, they have been adjusted by using relation (99): as shown from Fig. 9, a fairly good fit of these values is obtained (see Table 1 for the corresponding parameters).

6. Concluding remarks

In this work, the homogenisation method with multiple scale expansions was used to study the flow of incompressible generalised Newtonian fluids through porous media at low pore Reynolds numbers. The following points summarize the principal results of this study:

- A first-order equivalent macroscopic description was obtained from theoretical developments without any prerequisite at the macroscale: the resulting macroscopic flow is divergence free, and its momentum equilibrium is a balance between the macroscopic pressure gradient and a macroscopic volumetric viscous drag force characterizing the local fluid resistance.
- The viscous stress tensor of fluids under consideration can be expressed as the gradient of a viscous dissipation potential with respect to the local strain rate tensor. Whatever the considered porous medium, it was shown that such a property was preserved at the macroscale. Indeed, the macroscopic volumetric viscous drag force can be written as the gradient of the volume averaged local viscous dissipation potential, with respect to the volume averaged velocity field.
- This last property facilitates the formulation and the identification of macroscopic flow laws: this can be achieved by studying the evolution and the shape of isodissipations surfaces. Isodissipation surfaces can be built from permeation experiments by imposing to a given porous medium macrosopic pressure gradients (or macroscopic flows) with different orientations. They can also be identified from numerical simulation, as done in this work in the example of a 3D fibrous medium, by solving the self-equilibrium ((31a, 31c, 32c)) on a REV of this particular porous medium.
- Using the theory of anisotropic tensors functions, the general expressions of the macroscopic flow laws have then been further specified in cases of orthoropy, transverse isotropy and isotropy. Analytical phenomenological forms were also proposed to model isodissipation surfaces for such anisotropies, requiring a small number of additional constitutive parameters. Let us remark that other analytical expressions of v_{eq} (or f_{eq}) may be established, if necessary.
- In the case of the 3D orthotropic fibrous medium studied in this work, it was shown that (i) the proposed expressions fit numerical isodissipation surfaces rather well and (ii) most of the additional constitutive parameters could be linked with the microstructure, except the curvature parameters m_a, m_b and m_c, for which it was not possible to establish such correlations.

Efforts are now focusing on testing the capability of the proposed methodology to model the flow of generalised Newtonian fluids through more complex anisotropic porous media, such as woven fabrics and fibrous mats often involved in polymer composites.

References

[1] R.P. Chhabra, J. Comiti, I. Machac, Flow of non-Newtonian fluid in fixed and fluidized beds, Chem. Eng. Sci. 56 (2001) 1–27.
[2] A.O. Nieckele, M.F. Naccache, P.R.S. Mendes, Crossflow of viscoplastic materials through tube bundles, J. Non-Newtonian Fluid Mech. 75 (1998) 43–54.
[3] B.D. De Besses, A. Magnin, P. Jay, Viscoplastic flow around a cylinder in an infinite medium, J. Non-Newtonian Fluid Mech. 115 (2003) 27–49.
[4] P. Spelt, A. Yeow, C. Lawrence, T. Selerland, Creeping flows of Bingham fluids through arrays of aligned cylinders, J. Non-Newtonian Fluid Mech. 129 (2005) 66–74.
[5] K. Talwar, B. Khomani, Flow of viscoelastic fluids past periodic square arrays of cylinders: Inertial and shear thinning viscosity and elastic effects, J. Non-Newtonian Fluid Mech. 57 (1995) 177–202.
[6] A. Liu, D. Bornside, R. Armstrong, R. Brown, Viscoelastic flow of polymer solutions around a periodic, linear array of cylinders: Comparisons of predictions for microstructure and flow fields, J. Non-Newtonian Fluid Mech. 77 (1998) 153–190.
[7] H. Darcy, Les Fontaines Publiques de la Ville de Dijon, Victor Valmont, Paris, 1856.
[8] J. Pearson, P. Tardy, Models for flow of non-Newtonian and complex fluids through porous media, J. Non-Newtonian Fluid Mech. 102 (2002) 447–473.
[9] J.K. Woods, P.D.M. Spelt, P.D. Lee, T. Selerland, C.J. Lawrence, Creeping flows of power-law fluids through periodic arrays of elliptical cylinders, J. Non-Newtonian Fluid Mech. 111 (2003) 211–228.
[10] Z. Idris, L. Orgéas, C. Geindreau, J.-F. Bloch, J.-L. Auriault, Microstructural effects on the flow law of power-law fluids through fibrous media, Modelling Simul. Mater. Sci. Eng. 12 (2004) 995–1015.

[11] P.D.M. Spelt, T. Selerland, C.J. Lawrence, P.D. Lee, 'Flows of inelastic non-Newtonian fluids through arrays of aligned cylinders. Part 1. Creeping flows', J. Eng. Math. 51 (2005) 57–80.
[12] P.D.M. Spelt, T. Selerland, C.J. Lawrence, P.D. Lee, Flows of inelastic non-Newtonian fluids through arrays of aligned cylinders. Part 2. Inertial effects for square arrays, J. Eng. Math. 51 (2005) 81–97.
[13] L. Orgéas, Z. Idris, C. Geindreau, J.-F. Bloch, J.-L. Auriault, Modelling the flow of power-law fluids through anisotropic porous media at low pore Reynolds number, Chem. Eng. Sci. 61 (2006) 4490–4502.
[14] A. Bensoussan, J.-L. Lions, G. Papanicolaou, Asymptotic Analysis for Periodic Structures, North Holland, Amsterdam, 1978.
[15] E. Sanchez-Palencia, Non-homogeneous media and vibration theory, in Lectures Notes in Physics, vol. 127, Springer-Verlag, Berlin, 1980.
[16] H. Ene, E. Sanchez-Palencia, Equations et phénomènes de surface pourécoulement dans un modèle de milieu poreux, J. de Mécanique 14 (1975) 73–108.
[17] C.B. Shah, Y. Yortsos, Aspect of flow of power-law fluids in porous media, AIChE J. 41 (5) (1995) 1099–1112.
[18] A. Bourgeat, A. Mikelic, Homogenization of a polymer through a porous medium, Nonlinear Anal. Theory Meth. Appl. 26 (7) (1996) 1221–1253.
[19] J.-L. Auriault, P. Royer, C. Geindreau, Filtration law for power law fluids in anisotropic media, Int. J. Eng. Sci. 40 (2002) 1151–1163.
[20] J.-L. Lions, E. Sanchez-Palencia, Ecoulement d'un fluide viscoplastique de Bingham dans un milieux poreux, J. Math. Pures Appl. 60 (1981) 341–360.
[21] S. Whitaker, Advances in theory of fluid motion in porous media, Indus. Eng. Chem. 61 (1969) 14–28.
[22] S. Liu, J. Masliyah, On non-Newtonian fluid flow in ducts and porous media, Chem. Eng. Sci. 53 (1998) 1175–1201.
[23] S. Liu, J. Masliyah, Non-linear flow in porous media, J. Non-Newtonian Fluid Mech. 86 (1999) 229–252.
[24] G. Smit, J. du Plessis, Modelling of non-Newtonian purely viscous flow through isotropic high porosity synthetic foam, Chem. Eng. Sci. 54 (1999) 645–654.
[25] C. Tsakiroglou, A methodology for the derivation of non-darcian models for the flow of generalized Newtonian fluids in porous media, J. Non-Newtonian Fluid Mech. 105 (2002) 79–110.
[26] G. Smith, On isotropic functions of symmetric tensors skew-symmetric tensors and vectors, Int. J. Eng. Sci. 9 (1971) 899–916.
[27] J.-P. Boehler, A simple derivation of representations of non-polynomial constitutive equations in some cases of anisotropy, ZAMM 59 (1979) 157–167.
[28] I. Liu, On representations of anisotropic invariants, Int. J. Eng. Sci. 19 (1982) 1099–1109.
[29] J.-P. Boelher, Applications of Tensor Functions in Solid Mechanics CISM Courses and Lectures, Springer Verlag, Wien, NY, 1987.
[30] P. Carreau, D. DeKee, M. Daroux, An analysis of the behaviour of polymeric solutions, Can. J. Chem. Eng. 57 (1979) 135–140.
[31] K. Yasuda, R. Armstrong, R. Cohen, Shear-flow properties of concentrated-solutions of linear and star branched polystyrenes, Rheol. Acta 20 (1981) 163–178.
[32] G. Lipscomb, M. Denn, Flow of Bingham fluids in complex geometries, J. Non-Newtonian Fluid Mech. 14 (1984) 385.
[33] D. Gatling, N. Phan Tien, A numerical simulation of a plastic fluid in parallel-plate plastomer, J. Non-Newtonian Fluid Mech. 14 (1984) 347.
[34] T.C. Papanastasiou, Flow of materials with yield, J. Rheol. 31 (1987) 385–404.
[35] J.-L. Auriault, Heterogeneousmedium. is an equivalent description possible? Int. J. Eng. Sci. 29 (1991) 785–795.
[36] J. Lemaitre, J.-L. Chaboche, Mechanics of Solids Materials, Cambridge University Press, Cambridge, 1994.
[37] S.G. Advani, M.V. Bruschke, R.S. Parnas, Flow and Rheology in Polymer Composites Manufacturing—Resin Transfer Molding flow Phenomena in Polymeric Composites, Elsevier Science, 1994, Chapter 12. pp. 465–515.
[38] Comsol 2005. Reference manual, version 3.2. http://www.comsol.com.